A Spectral Boundary Element Method for Scattering Problems

J. Tausch[1] **and J. Xiao**[2]

Abstract: A fast method for the computation of layer potentials that arise in acoustic scattering is introduced. The principal idea is to split the singular kernel into a smooth and a local part. The potential due to the smooth part is discretized by a Nyström method and is evaluated efficiently using a sequence of FFTs. The potential due to the local part is approximated by a truncated series in the mollification parameter. The smooth approximation of the kernel is obtained by multiplication of its Fourier transform with a filter. We will show that for a rational filter the smooth part and the expansion coefficients of the local part can be found in closed form. The accuracy of the method is determined by the number of Fourier modes, the mollification parameter and the mesh width of discretization. We will investigate how to choose the parameters as a function of the wave number. The effectiveness of the method is illustrated for medium-sized scatterers (50–100 wavelengths) that may have complicated geometry.

Keywords: Boundary Element Method, Helmholtz Equation, Fast Method, Scattering

1   Introduction

It is commonly accepted that the boundary element method (BEM) is an effective approach to solve the Helmholtz equation in the exterior of a scatterer. It has the advantage that only the finite boundary surface has to be discretized and that the radiation condition is automatically satisfied. However, the conventional BEM typically leads to dense matrices, which makes the computational complexity prohibitive for large scale practical problems. In the recent past a variety of methods have been developed to handle this problem. These can be roughly classified into two groups, namely methods that are based on a hierarchical subdivision of space and grid-based methods.

[1] Southern Methodist University, Department of Mathematics, Dallas, TX, USA
[2] College of Astronautics, Northwestern Polytechnical University, Xi'an 710072, China

Examples of hierarchical methods are the fast multipole methodGreengard and Rokhlin (1987), hierarchical matricesBörm (2002); Bebendorf (2008), adaptive cross approximationBrancati and Aliabadi (2009) and waveletsBeylkin et al (1991). These methods place sources and evaluation points into a hierarchy of clusters. The efficiency and accuracy of these methods depends critically on how the cluster interactions can be approximated by low-rank matrices. In the case of boundary integral operators associated with the Laplace, Stokes or Lamé equations asymptotically optimal schemes have been developed. That is, the complexity of a matrix-vector multiplication is order $\mathcal{O}(N\log^{a}N)$ for some $a \geq 0$ (N is the degrees of freedom in the discretization), while the convergence rate of the discretization scheme is preserved, see, e.g. Sauter (2000); Tausch (2004).

In the case of the Helmholtz equation, the size of the scatterer, measured in wavelengths, is the dominant factor that influences computational cost and accuracy. It is well known that in the high-frequency regime large clusters in the coarse levels are no longer approximated by low-rank matrices, and therefore the efficiency of the aforementioned methods breaks down. To overcome this problem it has been proposed to use the fast multipole method with diagonal translation operators, Rokhlin (1990). This technique has been extended in Song et al (1998); Cheng et al (2005).

A different approach that avoids large clusters is to replace the surface distribution by equivalent sources on a uniform grid. The fast Fourier transform (FFT) can be employed to compute grid potentials efficiently. Since the grid is only accurate when the source and the evaluation point are well separated, the nearby interactions must be computed directly, by adding up contributions of individual sources. Grid-based methods are quite popular even though it appears that the asymptotic complexity is generally higher than what can be achieved with hierarchical methods. However, in many engineering applications the geometry is complicated and the mesh is relatively coarse, therefore small constant factors often play an important role Bespalov (2000). Applications of grid-based methods for the Laplace, Lamé and Helmholtz equations can be found in Hockney and Eastwood (1988); Phillips and White (1997); Fata (2008); Peirce and Napier (1995); Bruno and Kunyansky (2001).

If the scatterer is smooth and isomorphic to a sphere, spectral element methods, based on expansion of the solution into spherical harmonics have been shown to be successful Ganesh and Graham (2004). Papers for the efficient solution of multifrequency problems are Köhl and Rjasanow (2003); von Estorff et al (2005).

The approach described in this paper is more close to grid-based methods in that FFTs are used to accelerate the matrix-vector product. However, there is no uniform grid with equivalent charges. The idea here is to split the Green's function into a smooth approximation and a singular, essentially local part. The smooth part of the

Green's function is replaced by a rapidly converging Fourier series. We will show how a sequence of FFTs can be used to compute layer potentials with such a kernel effectively.

The local part is evaluated using a truncated Taylor series expansion with respect to the mollification parameter. Thus the computation of the local part amounts to multiplying with a diagonal matrix. Unlike the hierarchical or grid-based methods there is no need to compute and store singular surface integrals to account for nearby interactions of sources. Our numerical results demonstrate that the presented approach has short setup times and has low memory requirements. We believe that this is the main advantage of the presented method over the fast methods that appeared previously, because the computation of the nearfield interactions is usually a significant fraction of the overall solution cost.

For the heat equation the splitting of the Green's function into a smooth and a local part is obvious in that interactions with time steps in the past are smooth. Thus the history part can be expanded in a rapidly converging Fourier series. Furthermore, the recent time steps have a local kernel and allow an expansion in time. An algorithm based on such ideas was first discussed in Greengard and Strain (1990).

For the Helmholtz equation the way the Green's function is split into a smooth and a local part is not so clear: In Bespalov (2000) the singular part is replaced by a polynomial such that the resulting composite function is sufficiently smooth. The remainder is singular but local and is accounted for by computing individual panel interactions. This approach computes the distant interactions rapidly, but the treatment of the nearfield still involves the computation of weakly singular integrals which still contributes to a large constant in the complexity estimates.

In this paper we consider multiplying the Fourier transform of the kernel by a filter to obtain a smooth approximation. For the Laplace operator (i.e., vanishing wavenumber), a Gaussian filter results in a smooth part that can be expressed in closed form in spatial coordinates Tausch (2005). When the wavenumber is non-zero, this filter does not lead to closed-form expressions and is therefore not useful for numerical computations. In this article we show that a filter in the form of a rational function leads to a closed-form smooth part. We will discuss how the mollification parameter must depend on the wavenumber to ensure approximation. We will describe an algorithm that exploits the Fourier series expansion of the smooth part to compute the potential of a layer operator in order $N + s^3 \log s$ operations, where s is the number of Fourier modes. We conclude with several examples that illustrate the behavior of the method.

2   Problem Formulation

For simplicity of exposition, the focus of this paper will be on the sound-soft acoustic scattering of an incoming field u^{inc} of a smooth obstacle $D \subset \mathbf{R}^3$. The reflected field u is described by the Dirichlet problem to the Helmholtz equation with the Sommerfeld radiation condition

$$
\begin{aligned}
\Delta u(x) + \kappa^2 u(x) &= 0, \quad x \in \mathbb{R}^3 \setminus D \\
u(x) &= -u^{\text{inc}}(x), \quad x \in \Gamma := \partial D \\
\tfrac{\partial u}{\partial r} - i\kappa u &= \mathcal{O}(\tfrac{1}{|r|^2}).
\end{aligned}
\tag{1}
$$

Here, κ is the wave number, $|\cdot|$ denotes the Euclidean norm. We assume that the problem is scaled such that the scatterer is located inside a cube of side length $1 - d$, that is

$$
\Gamma \subset [0, 1-d]^3
\tag{2}
$$

where $0 < d \ll 1$ is a constant whose meaning will become clear in section 5.1.

A classical approach to treat the Helmholtz problem (1) is the combined layer ansatz of Brakhage and Werner Brakhage and Werner (1965), where the scattered field is represented by a combination of a single- and double layer potential

$$
u(x) = (\mathscr{K} - i\eta \mathscr{V})\sigma(x), \quad x \in \mathbb{R}^3 \setminus \overline{D},
\tag{3}
$$

where $\eta > 0$ is the coupling parameter, σ an unknown surface density and

$$
\mathscr{V}\sigma(x) := \int_\Gamma \frac{\exp(i\kappa|x-y|)}{4\pi|x-y|} \sigma(y)\, d\Gamma_y,
\tag{4}
$$

$$
\mathscr{K}\sigma(x) := \int_\Gamma \frac{\partial}{\partial n_y} \frac{\exp(i\kappa|x-y|)}{4\pi|x-y|} \sigma(y)\, d\Gamma_y
\tag{5}
$$

are the single and double layer operator, respectively. By letting $x \to \Gamma$ from the exterior of the scatterer, and taking the jump relations of layer potentials under consideration, the following boundary integral equation for σ can be derived

$$
\frac{1}{2}\sigma(x) + (\mathscr{K} - i\eta \mathscr{V})\sigma(x) = -u^{\text{inc}}(x), \qquad x \in \Gamma.
\tag{6}
$$

It is well known that (6) is a well posed problem when $\eta > 0$, see, e.g., Colton and Kress (1983).

3 Splitting of the Helmholtz Kernel

The method is based on splitting of the Helmholtz kernel

$$G = G_\delta^S + G_\delta^L \tag{7}$$

into a smooth part G_δ^S and a singular, local part G_δ^L. Here, δ is the mollification parameter that controls the smoothness of G_δ^S. Thus the single-layer potential is decomposed into

$$\mathcal{V} = \mathcal{V}_\delta^S + \mathcal{V}_\delta^L,$$

where the smooth and the local part of the single layer operator are

$$\mathcal{V}_\delta^S g(x) := \int_\Gamma G_\delta^S(x-y)g(y)\,d\Gamma_y, \tag{8}$$

$$\mathcal{V}_\delta^L g(x) := \int_\Gamma G_\delta^L(x-y)g(y)\,d\Gamma_y. \tag{9}$$

The splitting of the double layer potential $\mathcal{K} = \mathcal{K}_\delta^S + \mathcal{K}_\delta^L$ is defined analogously. To obtain the smooth part, we start with the following integral transform representation of the Helmholtz kernel

$$G(r) = \frac{\exp(i\kappa|r|)}{4\pi|r|} = \frac{1}{2\pi^2}\int_0^\infty \frac{\rho^2}{\rho^2 - \kappa^2}\, j_0(\rho|r|)\,d\rho. \tag{10}$$

Here $j_0(z) = \sin(z)/z$ is the spherical Bessel function of order zero. The integral in (10) is understood in the sense that the singularity at $\rho = \kappa$ is circumvented in the lower complex half-plane, thereby enforcing the Sommerfeld radiation condition. The imaginary part in the left hand side of (10) comes from integration along a complex path. Details of the derivation of (10) can be found in, e.g., Duffy (2001).

The decay rate of the integral transform at infinity determines the regularity of the kernel. The integrand in (10) decreases slowly as $\rho \to \infty$ which explains that the Green's function is singular in the origin. A smooth approximation of the kernel can be obtained by multiplying the transform with a filter which has a rapid decay rate at infinity. The resulting mollified Green's function is

$$G_\delta^S(r) = \frac{1}{2\pi^2}\int_0^\infty H\Big(\delta(\rho^2 - \kappa^2)\Big)\frac{\rho^2}{\rho^2 - \kappa^2}\, j_0(\rho|r|)\,d\rho \tag{11}$$

where H denotes the filter and δ is the mollification parameter. Since the integrand is singular for $\rho = \kappa$ it is more convenient to write the filter in the form as it appears in (11) and not as $H(\delta\rho^2)$. A natural choice of a filter a Gaussian, i.e., $H(z) = \exp(-z)$. For the Laplace equation (i.e., $\kappa = 0$) this was considered in

our previous work, see Tausch (2005). Unfortunately, for a nonzero frequency the mollified Green's function does not appear to have a closed form if a Gaussian filter is selected, and therefore we will consider a rational filter in the following.

To that end, write the filter in partial fractions decomposition

$$H(z) = \sum_{k=1}^{q} \frac{c_k}{z + w_k^2},$$ (12)

where the coefficients $w_k > 0$, $c_k \in \mathbb{C}$ and the regularity parameter q are at our disposition. To find a closed form of the integral in (11) we also need the partial fractions decomposition

$$\frac{H(z)}{z} = \sum_{k=0}^{q} \frac{d_k}{z + w_k^2}.$$ (13)

Basic complex variable arguments show that $w_0 = 0$ and

$$d_0 = H(0) \quad \text{and} \quad d_k = -\frac{c_k}{w_k^2}.$$ (14)

Substitution of (13) into (11) leads to

$$G_\delta^S(r) = \frac{1}{2\pi^2} \sum_{k=0}^{q} d_k \int_0^\infty \frac{\rho^2}{\rho^2 - \widehat{w}_k^2} j_0(\rho|r|) \, d\rho,$$

where

$$\widehat{w}_k = \sqrt{\kappa^2 - \frac{w_k^2}{\delta}}, \quad k = 0, \cdots, q.$$ (15)

The integrals in the last expression are of the same form as (10). Therefore the mollified Green's is given by

$$G_\delta^S(r) = d_0 \frac{\exp(i\kappa|r|)}{4\pi|r|} + \sum_{k=1}^{q} d_k \frac{\exp(i\widehat{w}_k|r|)}{4\pi|r|}.$$ (16)

Equation (16) represents a decomposition of $G(r)$ in a smooth and local part provided that $d_0 = 1$ and that the $\widehat{w}_k$'s have positive imaginary part. In this case the mollified Green's function consists of the original Green's function with some exponentially decreasing terms that remove the singularity at $r = 0$. Thus equations (14) and (15) imply the conditions on the filter,

$$H(0) = 1,$$ (17)

$$w_k > \sqrt{\delta}\kappa, \quad k = 1, \ldots, q.$$ (18)

Furthermore, it can be seen from (11) that if the filter satisfies

$$|H(t)| \le c \min\left(1, |t|^{-q}\right), \quad \text{for} - \delta\kappa^2 \le t < \infty \tag{19}$$

for some constant $c > 0$, then $G_\delta^S \in C^{2q+2}$.

If the filter satisfies (17), the local part is, up to a sign, the second term in (16). In the discussion below, it will be convenient to write $G_\delta^L(r)$ in the form

$$G_\delta^L(r) = -\sum_{k=1}^{q} d_k \frac{\exp(i\widehat{w}_k|r|)}{4\pi|r|} = \frac{1}{\sqrt{\delta}} E\left(\frac{|r|}{\sqrt{\delta}}\right) \tag{20}$$

where function E is given by

$$E(z) = -\sum_{k=1}^{q} d_k \frac{\exp(i\widetilde{w}_k z)}{4\pi z}, \tag{21}$$

and $\widetilde{w}_k = \sqrt{\delta}\widehat{w}_k$.

Filters that satisfy (17) and (19) can be found easily: choose real and mutually different roots $w_k \ne 0$, $k = 0, \ldots q$, and let

$$H(z) = \prod_{k=1}^{q} \frac{w_k^2}{z + w_k^2}. \tag{22}$$

Computing the partial fractions decomposition of the product shows that this filter is indeed of the form (12), with coefficients given by

$$c_k = w_k^2 \prod_{l \ne k} \frac{w_l^2}{w_l^2 - w_k^2}. \tag{23}$$

Figure 1 illustrates the behavior of the mollified Green's functions for various values of δ. The roots are $w_k = k$ and $q = 8$.

4 Expansion of the local operator

Since $E(z)$ is an exponentially decreasing function it is clear from (20) that $G_\delta^L(r)$ becomes more peaked and more rapidly decaying as δ decreases. Thus the potentials of the local operators $\mathcal{V}_\delta^L g(x)$ and $\mathcal{K}_\delta^L g(x)$ can be approximated using only the density at the evaluation point. In fact, we will show in this section that the expansions

$$\mathcal{V}_\delta^L g(x) = \delta^{\frac{1}{2}} \Phi_0 g(x) + \mathcal{O}(\delta^{\frac{3}{2}}), \tag{24}$$

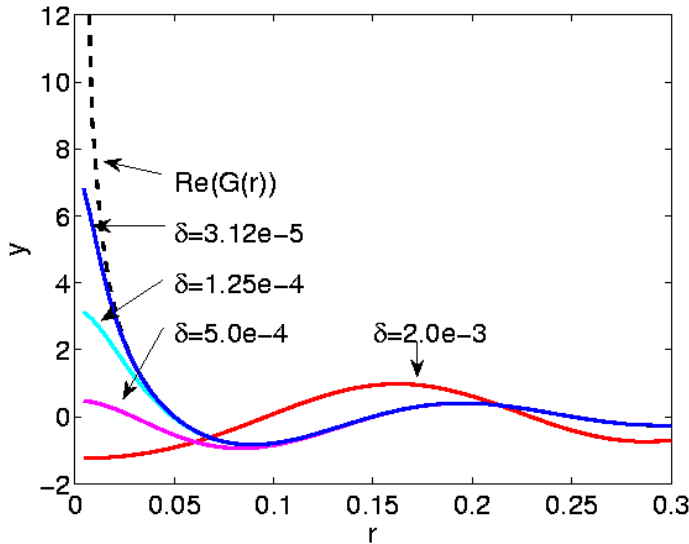$$\mathcal{K}_\delta^L g(x) = \delta^{\frac{1}{2}} \Psi_0(x) g(x) + \mathcal{O}(\delta^{\frac{3}{2}}) \tag{25}$$

Figure 1: The graph of the functions $y = \mathrm{Re}\,G(r)$ and $y = \mathrm{Re}\,G_\delta^S(r)$ for $\kappa = 10\pi$. The largest value δ=2e-3 does not satisfy condition (18) and therefore does not approximate G for large arguments.

hold for $\delta \to 0^+$. We will also determine the values for the coefficients Φ_0 and Ψ_0. To numerically compute the local potentials one can simply neglect the $\mathcal{O}(\delta^{\frac{3}{2}})$ remainder. Then the evaluation of the local part reduces to a multiplication with a diagonal matrix. It is also possible to obtain higher-order terms in the above expansions , using techniques developed for thermal layer potentials, see Tausch (2009). However, the discussion is technical and therefore we limit ourselves here to the first term.

To derive (24) and (25) for some point $x \in \Gamma$ we introduce a smooth cut-off function $\tilde{\chi}_v$ which is unity in the ball $\mathscr{B}_v(x)$, centered at x, and vanishes outside $\mathscr{B}_{2v}(x)$. The radius v is chosen to be small enough such that the piece of the surface inside $\mathscr{B}_{2v}(x)$ has a parameterization of the form $y(t) = x + Yt + n_x h(t)$. Here n_x is the normal of the surface at the point x, $Y \in \mathbb{R}^{3\times2}$ has two orthogonal columns that span the tangent plane at x and $h(t) = \mathcal{O}(|t|^2)$ is some scalar function in $t \in \mathbb{R}^2$.

The local single-layer potential $\mathscr{V}^{\mathrm{L}}_\delta$ in (9) can be written in the form

$$
\begin{aligned}
\mathscr{V}^{\mathrm{L}}_\delta g(x) &= \int_S G^{\mathrm{L}}_\delta(x-y)g(y)\,\mathrm{d}\Gamma_y \\
&= \frac{1}{\sqrt{\delta}}\int_S E\left(\frac{|x-y|}{\sqrt{\delta}}\right)\tilde{\chi}_v(x-y)g(y)\,\mathrm{d}\Gamma_y + R_\delta(x) \\
&= \frac{1}{\sqrt{\delta}}\int_{\mathbb{R}^2} E\left(\frac{|x-y(t)|}{\sqrt{\delta}}\right)\tilde{g}(t)d^2t + R_\delta(x).
\end{aligned}
\tag{26}
$$

Here, $E(\cdot)$ is defined in (21), $\tilde{g}(t) = \tilde{\chi}_v(x-y(t))g(t)J(t)$ where $J(t)$ is the Jacobian of the parameterization. The remainder $R_\delta(x)$ is the contribution from the exterior of $\mathscr{B}_v(x)$ which decays exponentially in $1/\delta$. Hence the remainder does not contribute to the series expansion at $\delta = 0$.

We assume that the function $h(t)$ in the parameterization of the surface is analytic, that is,

$$
h(t) = \sum_{|\alpha|\geq 2} h_\alpha t^\alpha.
\tag{27}
$$

Thus there are $\mathbb{C}^\infty$-functions H_n such that

$$
|x-y(t)| = |t|\sum_{n=0}^{\infty}|t|^n H_n(\hat{t})
\tag{28}
$$

where $\hat{t} := t/|t|$ and $H_0(\hat{t}) = 1$ and $H_1(\hat{t}) = 0$. Substituting (28) into (26) and changing variables $t \mapsto t/\sqrt{\delta}$ leads to

$$
\mathscr{V}^{\mathrm{L}}_\delta g(x) = \sqrt{\delta}\int_{\mathbb{R}^2} E\left(|t|\sum_{n=0}^{\infty}(\sqrt{\delta}|t|)^n H_n(\hat{t})\right)\tilde{g}(\sqrt{\delta}t)\,d^2t + R_\delta(x).
$$

The integral is an analytic function in $\sqrt{\delta}$ and can therefore be expanded in a Maclaurin series in $\sqrt{\delta}$. Substitution of $\sqrt{\delta} = 0$ into $\mathscr{V}^{\mathrm{L}}_\delta$ and $\frac{\partial}{\partial\sqrt{\delta}}\mathscr{V}^{\mathrm{L}}_\delta$ gives the first two terms in the series. We see that the zero-th order term is

$$
\Phi_0 = \int_{\mathbb{R}^2} E(|t|)d^2t = \frac{1}{2i}\sum_{k=1}^{q}\frac{d_k}{\tilde{w}_k}.
$$

and that the first order term vanishes because of the symmetry in the integrand. This establishes the validity of (24).

The local double layer potential is given by

$$
\begin{aligned}
\mathscr{K}^{\mathrm{L}}_\delta g(x) &= \int_S \frac{\partial}{\partial n_y}G^{\mathrm{L}}_\delta(x-y)g(y)\,\mathrm{d}\Gamma_y \\
&= -\frac{1}{\delta}\int_\Gamma E'\left(\frac{|x-y|}{\sqrt{\delta}}\right)\frac{(x-y)\cdot n_y}{|x-y|}g(y)\,\mathrm{d}\Gamma_y.
\end{aligned}
$$

The second factor of the kernel can be expanded in a similar manner as (28), we find that

$$\frac{(x-y) \cdot n_y}{|x-y|} = |t| \left(h_{02} \cos^2 \theta + h_{11} \cos \theta \sin \theta + h_{20} \sin^2 \theta\right) + \mathcal{O}(|t|^2)$$

where θ is the angular coordinate of t and the h's are from expansion (27). Proceeding in a similar manner as for the single layer operator leads to the expansion (25), where

$$\Psi_0(x) = (h_{02} + h_{20}) \frac{1}{2i} \sum_{k=1}^{q} \frac{d_k}{\tilde{w}_k}.$$

The expression $(h_{02} + h_{20})$ is the mean curvature of the surface at the point x.

If the surface is only piecewise smooth, and x is on an edge or vertex of the surface, the parameterization $y(t)$ must be defined for every face that contains x, which will lead to expansions similar to (24) and (25).

5   Fast algorithm for the smooth part

If the higher order terms in the expansion of the local part are truncated, integral equation (6) becomes

$$\lambda_\delta(x)\sigma_\delta(x) + (\mathscr{K}_\delta^S - i\eta \mathscr{V}_\delta^S)\sigma_\delta(x) = -u^{\mathrm{inc}}(x), \qquad x \in \Gamma. \tag{29}$$

where

$$\lambda_\delta(x) = \frac{1}{2} + \delta^{\frac{1}{2}}\left(\Psi_0(x) - i\eta \Phi_0\right)$$

Since the integral operators have smooth kernels the Nyström method is the simplest discretization option. Here, the integral is replaced by a surface quadrature rule of the form

$$\int_\Gamma f(y) d\Gamma_y \approx \sum_{j=1}^{N} f(x_j) w_j,$$

where $x_i \in \Gamma$ are the nodes and w_i are the weights of the quadrature rule. The construction of such a quadrature rule begins with a subdivision of the surface in triangular patches of maximal diameter h. The nodes and weights are chosen such that the quadrature rule is exact for polynomials of a given degree. Since the domain of integration is a two-dimensional manifold the number of nodes scales like $N = O(h^{-2})$. Details can be found in many references, such as Atkinson (1997). The

discretization of the layer potentials is

$$\mathcal{V}^{\mathrm{S}}_{\delta,h} g(x) := \sum_{j=1}^{N} G^{\mathrm{S}}_{\delta}(x - x_j) g(x_j) w_j, \tag{30}$$

$$\mathcal{K}^{\mathrm{S}}_{\delta,h} g(x) := \sum_{j=1}^{N} \frac{\partial}{\partial n_j} G^{\mathrm{S}}_{\delta}(x - x_j) g(x_j) w_j. \tag{31}$$

The Nyström discretization replaces the integral operators by their discrete counterparts and enforces equation (29) at the node points of the quadrature. The result is the linear system

$$\lambda_{\delta}(x_i)\sigma_{\delta,h}(x_i) + (\mathcal{K}^{\mathrm{S}}_{\delta,h} - i\eta \mathcal{V}^{\mathrm{S}}_{\delta,h})\sigma_{\delta,h}(x_i) = -u^{\mathrm{inc}}(x_i), \qquad i = 1, \ldots, N. \tag{32}$$

We describe a fast algorithm for evaluating the smooth part of the combined layer operator, which is based on replacing the smooth kernel G^S_{δ} by a truncated Fourier series. For rapid convergence it is necessary to multiply this kernel with a sufficiently smooth cut-off function χ that is unity inside the cube $[-1+d, 1-d]^3$ and vanishes outside $[-1, 1]^3$. Since we assumed in (2) that the surface is contained in $[0, 1-d]^3$, the cut-off function has no effect on the integral, thus the smooth part of the combined layer is given by

$$
\begin{aligned}
u^{\mathrm{S}}(x) &:= \left(\mathcal{K}^{\mathrm{S}}_{\delta,h} - i\eta \mathcal{V}^{\mathrm{S}}_{\delta,h} \right) g(x) \\
&= \sum_{j=1}^{N} \left(\frac{\partial}{\partial n_y} - i\eta \right) \left(\chi G^{\mathrm{S}}_{\delta} \right)(x - x_j) g(x_j) w_j, \quad x \in \Gamma.
\end{aligned} \tag{33}
$$

In the fast algorithm the kernel $\chi G^{\mathrm{S}}_{\delta}$ is approximated by the truncated Fourier series G_s

$$G_s(r) := \sum_{\|\omega\|_{\infty} \leq s} \widehat{G}_{\omega} \exp(i\pi\omega \cdot r), \quad r \in [-1, 1]^3 \tag{34}$$

where the summation index ω is in $\mathbb{Z}^3$ and $\widehat{G}_{\omega}$ is a Fourier coefficient of $\chi G^{\mathrm{S}}_{\delta}$, given by

$$\widehat{G}_{\omega} = \frac{1}{8} \int_{[-1,1]^3} \exp(-i\pi\omega \cdot r) \left(\chi G^{\mathrm{S}}_{\delta} \right)(r) \, \mathrm{d}^3 r. \tag{35}$$

The resulting approximate potential is a truncated Fourier series

$$u^{\mathrm{S}}_s(x) := \sum_{j=1}^{N} \left(\frac{\partial}{\partial n_j} - i\eta \right) G_s(x - x_j) g(x_j) w_j = \sum_{\|\omega\|_{\infty} \leq s} \exp(i\pi\omega \cdot x) \widehat{d}_{\omega} \tag{36}$$

where $\widehat{d}_\omega = \widehat{G}_\omega \widehat{g}_\omega$ and

$$\widehat{g}_\omega = \sum_{j=1}^{N} \left(\frac{\partial}{\partial n_y} - i\eta \right) \exp(-i\pi\omega \cdot x_j) g(x_j) w_j. \tag{37}$$

In summary, the potential computation of the potential due to the smooth parts consists of three stages.

1. Compute the Fourier coefficients $\widehat{g}_\omega$ in (37).

2. Multiply $\widehat{d}_\omega := \widehat{G}_\omega \widehat{g}_\omega$ for $\|\omega\|_\infty \leq s$.

3. Evaluate the Fourier series (36) for $x \in \Gamma$.

The Fourier coefficients in Stage 1 are computed by a sequence of FFTs, which will be described in Section 5.1 . Stage 3 consists of another sequence of FFTs which will be discussed in Section 5.2. Stage 2 obviously involves $\mathcal{O}(s^3)$ operations. The choice of s and the other parameters will be discussed in Section 6.

5.1   Computation of the $\widehat{g}_\omega$'s

In this section we describe how FFTs can be used to efficiently compute the Fourier coefficients of the function g. To that end, the three-space is divided into cubes C_l, $l = (l_1, l_2, l_3) \in \mathbb{Z}^3$. These cubes have centers $\bar{x}_l = (l_1, l_2, l_3)/s$ and side length $1/s$. Note that s is the same as in (34) and therefore the cubes get smaller if more terms in the Fourier series expansion of the Green's function are retained. Because of assumption (2) Γ is contained in the union the cubes with indices $0 \leq l_j < s$, provided that $d \geq 1/(2s)$. The piece of the surface that intersects with the l-th cube is denoted by $\Gamma_l = \mathscr{C}_l \cap \Gamma$ and the set of quadrature nodes that is located on Γ_l is denoted by $\mathscr{I}_l$, c.f. Figure 2.

From (37) it follows that the Fourier coefficients of g can be written as

$$\widehat{g}_\omega = \sum_{\|l\|_\infty \leq s} \exp\left(\frac{-i\pi\omega \cdot l}{s} \right) \sum_{j \in \mathscr{I}_l} \left(\frac{\partial}{\partial n_j} - i\eta \right) \exp\left(-i\pi\omega \cdot (x_j - \bar{x}_l)\right) g(x_j) w_j. \tag{38}$$

The frequency and the spatial variable in the sum can be separated using the Jacobi-Anger expansion, which is normally stated as

$$\exp(-i\xi t) = \sum_{v=0}^{\infty} (-i)^v (2v+1) j_v(\xi) P_v(t), \qquad -1 \leq t \leq 1,$$

see, e.g., Nédélec (2001). Here, $j_v(\cdot)$ is the spherical Bessel function of order v and $P_v(\cdot)$ is the Legendre polynomial of degree v. This formula generalizes to the
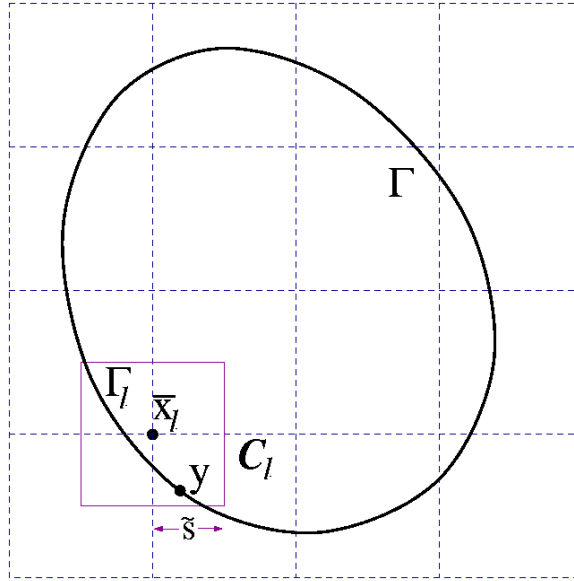
Figure 2: Two dimensional illustration of the geometry. The cube C_{11} is highlighted.

three-variate case and can be applied to the exponential in the sum of (38)

$$\exp(-i\pi\omega \cdot (x_j - \bar{x}_l)) \approx \sum_{|\alpha| \leq p} (-i)^{|\alpha|} (2\alpha + 1) j_\alpha(\pi\tilde{s}\omega) P_\alpha \left(\frac{x_j - \bar{x}_l}{\tilde{s}} \right) \tag{39}$$

where p is the expansion order, $\tilde{s} = 1/(2s)$ is the half-length of a small cube, $\alpha = (\alpha_1, \alpha_2, \alpha_3)$ is a multi-index, $|\alpha| = \alpha_1 + \alpha_2 + \alpha_3$, $j_\alpha(x) = j_{\alpha_1}(x_1) j_{\alpha_2}(x_2) j_{\alpha_3}(x_3)$ and $P_\alpha(x)$ is defined similarly. Substitution of (39) into (38) leads to the approximation

$$\hat{g}_\omega \approx \sum_{|\alpha| \leq p} (-i)^\alpha (2\alpha + 1) j_\alpha(\pi\tilde{s}\omega) \sum_{\|l\|_\infty \leq s} \exp \left(\frac{-i\pi\omega \cdot l}{s} \right) m_l^\alpha(g),$$

where $m_l^\alpha(g)$ is the moment

$$m_l^\alpha(g) = \sum_{j \in \mathscr{I}_l} \left(\frac{\partial}{\partial n_y} - i\eta \right) P_\alpha \left(\frac{x_j - \bar{x}_l}{\tilde{s}} \right) g(x_j) w_j. \tag{40}$$

To write the above computation in matrix form, we define the matrices $M_r(\alpha)$ for

$r \in \{0,1\}$ by their coefficients

$$[M_r(\alpha)]_{l,j} = \begin{cases} \left(\frac{\partial}{\partial n_y} - i\eta\right)^r P_\alpha\left(\frac{x_j - \bar{x}_l}{\tilde{s}}\right) & \text{if } x_j \in \mathscr{I}_l, \\ 0 & \text{otherwise.} \end{cases} \tag{41}$$

Furthermore, $K(\alpha)$ denotes the diagonal matrix

$$K(\alpha) = \text{diag}\left((-i)^{|\alpha|}(2\alpha+1)j_\alpha(\pi\tilde{s}\omega), \|\omega\|_\infty \leq s\right). \tag{42}$$

Using these notations, the (approximate) coefficient vector $\widehat{g}$, consisting of $\widehat{g}_\omega$'s, is given by

$$\widehat{g} = \sum_{|\alpha| \leq p} K(\alpha) F M_1(\alpha)\vec{g}, \tag{43}$$

where F is the $2s$-long three-dimensional discrete Fourier transform and $\vec{g}$ the vector with components $g(x_j)w_j$. There are $(p+1)(p+2)(p+3)/6$ terms in the above sum. The choice of p is determined by convergence of the Jacobi-Anger expansion. Since by design of the algorithm

$$\tilde{s}\|\omega\|_\infty \leq \frac{1}{2},$$

hence the argument to the Bessel function in (39) is small and independent of all parameters. Therefore a small value of p will suffice.

5.2 *Evaluation of the Fourier series*

We now turn to the evaluation of the potentials $u_s^S(x_i)$ in (36), assuming that the coefficients $\widehat{d}_\omega$ have been computed. In order to evaluate this potential efficiently, the Jacobi-Anger approximation (39) is used again, in a very similar manner as in the previous section. Specifically, let l be the index of the cube $\mathscr{C}_l$ that contains the node point x_j, then

$$u_s^S(x_j) = \sum_{\|\omega\|_\infty \leq s} \exp\left(\frac{\pi i\,\omega \cdot l}{s}\right)\exp\left(i\pi\omega(x_j - \bar{x}_l)\right)\widehat{d}_\omega$$

$$\approx \sum_{|\alpha| \leq p}\sum_{\|k\|_\infty \leq s}\exp\left(\frac{i\pi\omega \cdot l}{s}\right)i^{|\alpha|}(2\alpha+1)j_\alpha(\pi\tilde{s}\omega)P_\alpha\left(\frac{x_j - \bar{x}_l}{\tilde{s}}\right)\widehat{d}_\omega,$$

In matrix notation, the evaluation of the Fourier series is

$$\vec{u} = \sum_{|\alpha| \leq p} M_0(\alpha)^T F^* K^*(\alpha)\vec{d}, \tag{44}$$

where $M_0(\alpha)$ and $K(\alpha)$ are the matrices defined in (41) and (42), respectively, and $\vec{d}$ consisting of $\widehat{d}_\omega$'s.

5.3 *Evaluation the Fourier coefficients of the Kernel*

The Fourier coefficients of the smooth kernel are computed just like the coefficients of the density. From (35) it follows that

$$\widehat{G}_\omega = \frac{1}{8} \sum_{\|l\|_\infty \le s} \exp\left(\frac{-i\pi\omega \cdot l}{s}\right) \int_{\mathscr{C}_l} \exp(-i\pi\omega \cdot (y - x_l))(\chi G_\delta^S)(y) \, d\Gamma_y. \tag{45}$$

The Jacobi-Anger expansion leads to

$$\widehat{G} = \sum_{|\alpha| \le p} K(\alpha) F \, \check{m}_\alpha \tag{46}$$

where the moments

$$\check{m}_l^\alpha = \frac{1}{8} \int_{\mathscr{C}_l} P_\alpha\left(\frac{y - x_l}{\tilde{s}}\right)(\chi G_\delta^S)(y) \, d^3y$$

are computed using high-order Gauss quadratures.

6 Choice of parameters and Complexity

This section presents a rationale for choosing the mollification parameter δ, the number of Fourier modes s in (36) and the mesh width of the Nyström quadrature rule as a function of the wavenumber κ.

Recall that condition (18) is necessary to ensure that $G_\delta^L(r)$ is indeed a local function. If the filter (and therefore, w_k) is fixed as $\kappa \to \infty$, then the relationship

$$\delta\kappa^2 = \tilde{\kappa}^2 \tag{47}$$

must hold for a fixed $\tilde{\kappa} < \min_k w_k$. After the change of variables $\tilde{\rho} = \sqrt{\delta}\rho$ the integral representation of the smooth part (11) is

$$G_\delta^S(r) = \frac{1}{2\pi^2\sqrt{\delta}} \int_0^\infty H(\tilde{\rho}^2 - \tilde{\kappa}^2) \frac{\tilde{\rho}^2}{\tilde{\rho}^2 - \tilde{\kappa}^2} j_0\left(\tilde{\rho}\frac{|r|}{\sqrt{\delta}}\right) d\tilde{\rho} = \frac{1}{\sqrt{\delta}} \tilde{G}_\delta^S\left(\frac{r}{\sqrt{\delta}}\right),$$

where $\tilde{G}_\delta^S$ is a fixed function, independent of the wave number. Because of the scaling in the last equation, the mesh width in the Nyström discretization must be proportional to $\sqrt{\delta}$ in order to resolve the peak of $G_\delta^S(r)$ near $r = 0$. For the same reason, the number of Fourier modes in (36) must be proportional to $1/\sqrt{\delta}$. Because of (47) we see that

$$N \sim h^{-2} \sim \kappa^2 \quad \text{and} \quad s \sim \kappa. \tag{48}$$

The computation of the vectors $\widehat{g}$ in (43) involves the application of the matrices $M_1(\alpha)$ and $K(\alpha)$ at a cost of N and $(2s)^3$ operations, repectively. Furthermore the cost of an FFT is $\frac{3}{2}\log(s)(2s)^3$. Since there are $(p+1)(p+2)(p+3)/6$ terms in the sum of (43) the total cost of computing the vector $\widehat{g}$ is $\frac{p^3}{6}(12\log(s)s^3 + N)$ operations (neglecting the lower order terms). The matrix for the computation of the vector $\vec{u}$ in (44) is the adjoint of the matrix in (43), hence the computational cost is the same. The cost of the multiplication with the $\widehat{G}_\omega$'s is of lower order.

As discussed in section 5.1, the parameter p is a constant, thus the cost of a matrix-vector product under the assumption of (48) is $O(\kappa^3 \log \kappa)$.

7   Numerical Examples

We have implemented the method and tested its effectiveness on various scatterers. For the smooth part, we use filter (22) with $q = 8$, $w_k = k$ and c_k given by (23). Increasing q or replacing the filter by another one that satisfies the assumptions had little effect on the overall performance of the algorithm. The truncation parameter of the Jacobi-Anger expansion in (39) is always set to $p = 4$. The quadrature rule in the Nyström method is the midpoint rule for surface integrals. That is, the surface is triangulated by flat triangles, the quadrature nodes are the centers of the triangles and the weights are their areas. The FFTs are done by FFTW Johnson (2005), the code is compiled with gcc with optimization turned on. The CPU is a 2.4 Ghz AMD Opteron processor. The system's eight gigabyte memory was sufficient to run all examples in core.

7.1   Sphere

In the first example involves computing the farfield pattern when the unit sphere is hit with a plane wave. The farfield is computed from the density using the formula

$$\alpha(\widehat{x}) = i \int_\Gamma \exp(-i\kappa\widehat{x} \cdot y)(\eta + \kappa\widehat{x} \cdot n_y)\sigma(y) \, d\Gamma_y, \quad \widehat{x} \in \mathbb{S},$$

see, e.g., Nédélec (2001). Since Γ is a sphere, the solution σ as well as the farfield can be expressed in closed form. The coupling parameter in (3) is $\eta = \kappa/2$ and the linear system is solved with GMRES without any preconditioning. In these experiments the sphere is initially triangulated by a coarse mesh, then the mesh is uniformly refined each time the frequency is doubled. Likewise, the order of the highest Fourier mode s in (34) is doubled each time the frequency is doubled. The mesh width is proportional to the wavelength and the number of panels N is quadrupled with every mesh refinement. With a given combination of κ, N and s there is a trade-off when choosing the parameter δ. If δ is small the mollified Green's function is more peaked which implies that the truncation error of the Fourier series is

large. If δ is large, the expansion error of the local part in (24) and (25) is large. This is illustrated in Figure 3 which plots the error for the discretization parameters in Table 1.
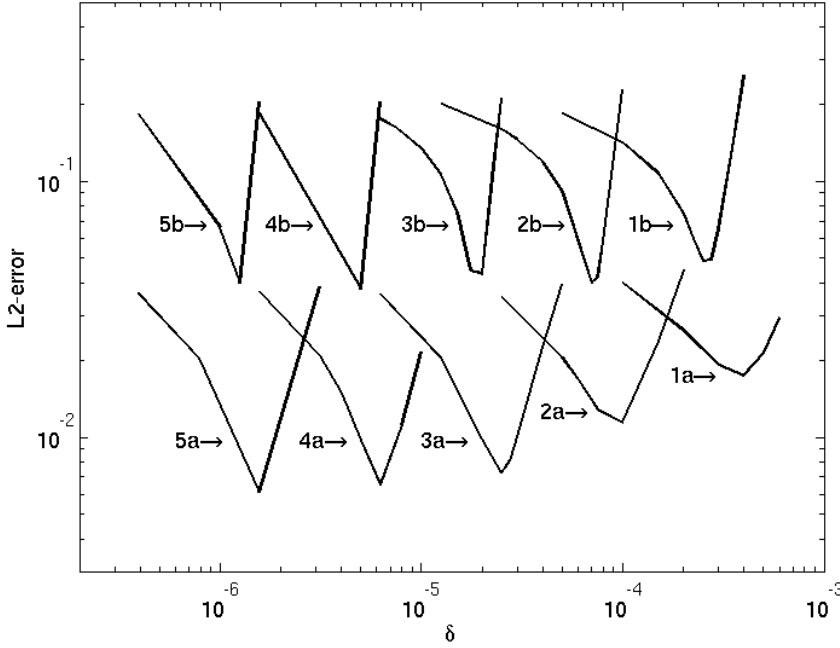

Figure 3: Relative $L^2(\mathbb{S})$-error of the farfield of the sphere as a function of δ for the parameters given in Table 1

.

The results shown in the figure are in good agreement with (47), that is, $\delta \sim 1/\kappa^2$. In fact, when the frequency is doubled, the optimal value of δ is reduced by the factor four. Furthermore, the error stays about the same when κ is increased and $s \sim \kappa$ and $\delta \sim 1/\kappa^2$.

The timings displayed in Table 1 are the time per iteration and the total time, which also includes the time to compute the Fourier coefficients $\widehat{G}_k$. Since the time per iteration and setup are independent of δ, we only list the time for the optimal δ. The number of GMRES iterations is somewhat dependent on κ and δ, we display iteration counts only for the optimal δ. The time per iteration increases by a factor somewhat larger than eight when doubling the wavenumber, which agrees well

Label	N	s	size in wavelengths	its	mem (MB)	time/itr (sec)	time (sec)
1a	5120	16	3.13	9	8.3	0.1	3
2a	20480	32	6.25	11	34.2	1.6	27
3a	81920	64	12.5	13	145.4	15.3	288
4a	327680	128	25	15	623.9	127.4	2523
5a	1310720	256	50	18	3071	1189	26161
1b	1280	16	6.25	11	2.3	0.1	3
2b	5120	32	12.5	13	9.7	0.8	25
3b	20480	64	25	16	45.0	13.2	290
4b	81920	128	50	19	230.6	116.8	2829
5b	327680	256	100	23	1323	1130	30755

Table 1: Parameters and timings for the sphere. Top: Lower frequency with higher accuracy. Bottom: Higher frequency with lower accuracy.

with the $\kappa^3 \log \kappa$ complexity estimate. The code stores the Fourier coefficients $\widehat{G}_k$ and $\widehat{g}_k$, the moments $m^\alpha(g)$, as well as the orthogonal basis of the Krylov subspace generated by GMRES. For the size of problems computed, the Krylov basis consumes the largest portion of the overall memory usage. Since this part grows roughly like κ^2, the growth rate of the overall storage appears slower in the table than the actual asymptotic estimate.

7.2 Disk backed by a Ground plane

We now test the performance of the algorithm on an infinitely thin disk, $\{(x,y,0.1), x^2 + y^2 \leq 0.25\}$, which is backed by an infinite plane at $z = 0$. The incoming field

$$u^{\text{inc}}(x,y,z) = \exp\left(i\kappa(\cos(\varphi)x)\right)\sin(\kappa\sin(\varphi)z)$$

represents a plane wave that approaches the plane $z = 0$ at an angle φ and its reflected wave. The source density of this problem are shown in Figure 4 and the scattered fields in Figure 5. To compute the field that is scattered from the disk we use the method of images, i.e., we place an identical disk at $z = -0.1$. Since the scatterer has no interior, there are no spurious resonances, and therefore it is sufficient to solve the problem with the single layer potential equation $\mathscr{V}\sigma = -u^{\text{inc}}$. Since the resulting charge density is singular on the edges of the disk, we use a graded mesh that is refined where we expect the singularity.

Since this problem has no analytical solution we investigate the convergence of the solution when refining the discretization parameters. Figures 4 display the real part
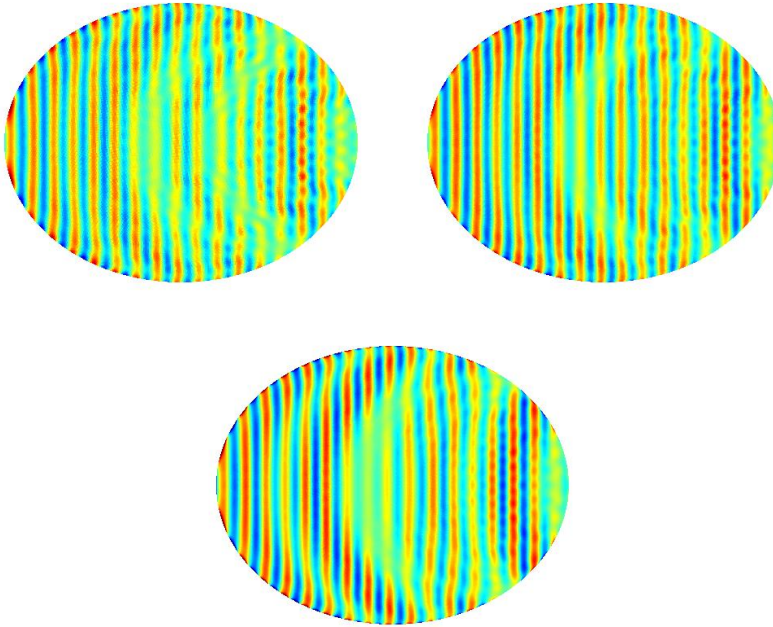
Figure 4: Three refinements (left: coarse, right: finer, bottom: finest) of the real part of the source density for the disk, 17 wavelenghts

of the source density on the disk for the discretization parameters shown in Table 2. There are some apparent differences between the first and second mesh, but it is hard to see differences between the second and third mesh. The singular behavior is hard to spot in the figures, because the density grows large only very close to the edge.

While we observed rapid convergence of the iterative solver in the sphere example, the convergence in the disk example is much slower. A side effect is the increased memory allocation to store the orthogonal basis of the Krylov subspace in the GM-RES algorithm, since we do no restarts. This accounted for approximately sixty percent of the overall memory allocation. We did not precondition the linear system, but note that there are numerous preconditioners that are effective for integral formulations of scattering problems, see Carpentieri (2006), which could be used here.
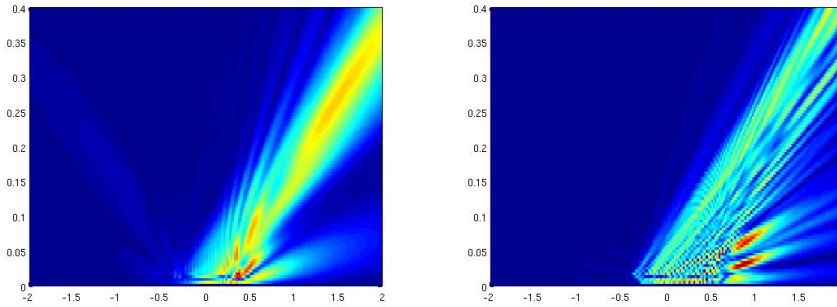
Figure 5: Scattered field of the disk. Low Frequency(left, 8.5 wavelenghts) and high Frequency, (34 wavelenghts right)

N	s	size in wavelengths	δ	its	mem (MB)	time/itr (sec)	time (sec)
130048	64	17	1.25×10^{-5}	64	310	15.3	1072
520192	128	17	3.125×10^{-6}	67	1286	126	9172
2080768	256	17	7.8125×10^{-7}	82	5528	1102	95871
32512	32	8.5	5.0×10^{-5}	68	76	1.6	123
520192	128	34	3.125×10^{-6}	100	1286	126	13296

Table 2: Disk example. Top: Parameters used to obtain the densities shown in Fig. 4. Bottom: Parameters used to obtain the fields shown in Fig. 5

7.3 Airplane

To illustrate that the technique discussed in this paper can be used for very general scatterers we include the Boeing 747 example shown in Figure 6. The surface of the airplane is assumed to be sound soft. The geometry is discretized into 556552 triangular panels, and no further information, such as parameterizations, are known.

Figure **??** compares the scattering amplitude for $s = 128$ and $s = 256$ Fourier modes. Since it is hard to spot differences in the two solutions, it appears that already the smaller value of s will give an acceptable accuracy in many applications. The size of the scatterer in this problem is about 45 wavelengths, the memory allocation of the smaller problem is 906MB and the CPU time is 4355 seconds.

Figure 8 displays the density for 90 wavelengths and $s = 256$. The memory allocation is 1583 MB and the CPU time is 36361 seconds.

Figure 6: 3D rendering of the airplane.

8   Conclusions

We have presented a method for the computation of scattered fields that has order $\kappa^3 \log \kappa$ complexity when the mesh width is proportional to the wavelength. Since $N \sim \kappa^2$ the asymptotic estimate is not optimal, but because of small constants we have been able to solve scatterers of one hunderd wavelenghts in eight to nine hours. Most of the CPU time is spent evaluating the sums in (43) and (44). Since this part is embarrassingly parallel one can expect almost optimal speed up on distributed memory multiprocessor machines. In our implementation the surface of the scatterer is given in terms of a triangulation, and the curvature in (24) is approximated by finite differences. If more information about the surface is known, e.g., if it is given by parameterizations, then one could compute more terms in the expansion of the local part and obtain higher order schemes. However, in many realistic situations the surface is not known to such precision, such as in the case of a triangulation. The point of the airplane expample is to demonstrate that the presented algorithm is robust in this situation. In the case of sound-hard scattering the combined integral equation involves the hypersingular integral. This operator can be treated with our methodology if it is rewritten in the curl-curl form, see e.g. **?**. However, the details are somewhat technical and we will consider this in our future work.
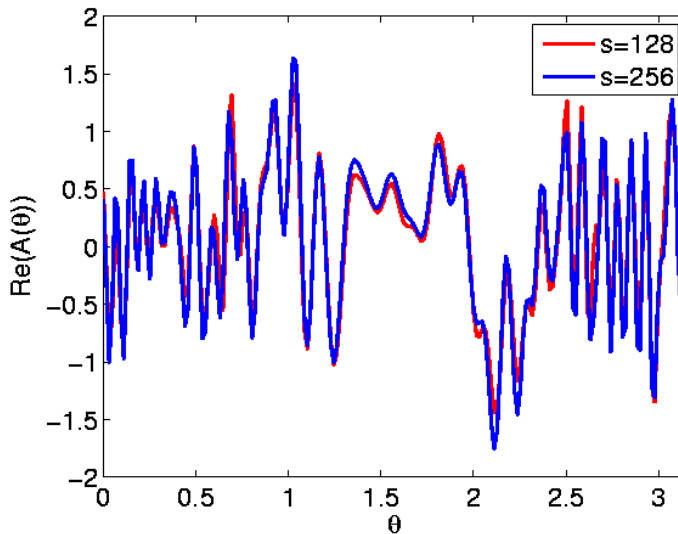
Figure 7: Comparison of the scattering amplitude as a function of θ (setting $\varphi = 0$ for two different discretizations. 45 wavelengths

9   Acknowledgment

References

Atkinson, K. E. (1997): *The Numerical Solution of Integral Equations of the Second Kind*, Cambridge University Press.

Bebendorf, M. (2008): *Hierarchical Matrices: A Means to Efficiently Solve Elliptic Boundary Value Problems*, Springer.

Bespalov, A. (2000): On the use of a regular grid for implementation of boundary integral methods for wave problems, *Russ. J. Numer. Anal. Math. Modelling* 15 (6), 469–488.

Beylkin, G.; Coifman, R.; Rokhlin, V. (1991): Fast wavelet transforms and numerical algorithms, *Comm. Pure Appl. Math.* XLIV, 141–183.

Börm, S.; Grasedyck, L.; Hackbusch, W. (2002): Introduction to hierarchical matrices with applications, *Engrg. Anal. Boundary Elements*, 405–422.
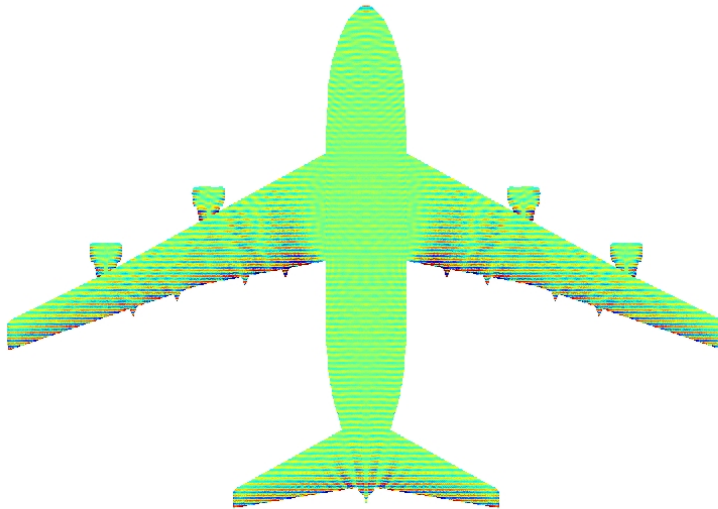
Figure 8: The density (imaginary part) for 90 wavelengths

Brakhage, H.; Werner, P. (1965): über das Dirichletsche Aussenraumproblem für die Helmholtzsche Schwingungsgleichung, *Arch. Math.* 16, 325–329.

Brancati, I. B. A.; Aliabadi, M. H. (2009): Hierarchical adaptive cross approximation gmres technique for solution of acoustic problems using the boundary element method, *CMES: Comput. Model. Engrg Sci.* 43 (2), 149–172.

Bruno, O.; Kunyansky, L. (2001): A fast, high-order algorithm for the solution of surface scattering problems: Basic implementation, tests, and applications, *J. Comput. Phys.* 169 (1), 80–110.

Carpentieri, B. (2006): Combining fast multipole techniques and an approximate inverse preconditioner for large electromagnetism calculations, *SIAM J. Sci. Statist. Comput.* 27, 774–792.

Cheng, H.; Crutchfield, W. Y.; Gimbutas, Z.; Greengard, L.; Ethridge, J.; Huang, J. (2005): A wideband fast multipole method for the helmholtz equation in three dimensions, *J. Comput. Phys.* 216, 300–325.

Colton, D.; Kress, R. (1983): *Integral Equation Methods in Scattering Theory*, Wiley, New York.

Duffy, D. (2001): *Green's Functions with Applications*, Chapman and Hall/CRC.

Fata, S. (2008): Fast Galerkin BEM for 3D potential theory, *Comput. Mech.* 42, 417–429.

Ganesh, M.; Graham, I. (2004): A high-order algorithm for obstacle scattering in three dimensions, *J. Comput. Phys.* 198, 211–242.

Greengard, L.; Rokhlin, V. (1987): A fast algorithm for particle simulations, *J. Comput. Phys.* 73, 325–348.

Greengard, L.; Strain, J. (1990): A fast algorithm for the evaluation of heat potentials, *Comm. Pure Appl. Math.* XLIII, 949–963.

Hockney, R. W.; Eastwood, J. W. (1988): *Computer Simulations using Particles*, McGraw-Hill, New York.

Johnson, M. F. S. (2005): The design and implementation of FFTW3, *Proceedings of the IEEE* 93 (2), 216—231, special issue on "Program Generation, Optimization, and Adaptation".

Köhl, M.; Rjasanow, S. (2003): Multifrequency analysis for the helmholtz equation, *Comput. Mech.* 32 (4–6), 234–239.

Nédélec, J.-C. (2001):*Acoustic and Electromagnetic Equations*, Springer.

Peirce, A.; Napier, J. (1995): A spectral multipole method for efficient solution of large-scale boundary element models in elastostatics, *Internat. J. Numer. Methods Engrg.* 38, 4009–4034.

Phillips, J.; White, J. (1997): A precorrected-FFT method for electrostatic analysis of complicated 3-D structures, *IEEE Trans. Circuits and Systems* 16 (10) 1059–1073.

Rokhlin, V. (1990): Rapid solution of integral equations of scattering theory in two dimensions, *J. Comput. Phys.* 86, 414–439.

Sauter, S. (2000): Variable order panel clustering, *Computing* 64 (3), 223–277.

Song, J.; Lu, C.; Chew, W.; Lee, S. (1998): Fast Illinois solver code FISC, *IEEE Antennas Propag. Mag.* 40, 27–34.

Tausch, J. (2004): The variable order fast multipole method for boundary integral equations of the second kind, *Computing* 72 (3), 267–291.

Tausch, J. (2005): A spectral method for the fast solution of boundary integral formulations of elliptic problems, in: Constanda, C.; Nashed, Z.; D. Rollins (Eds.), *Integral Methods in Science and Engineering*, Birkhauser, pp. 289–297.

Tausch, J. (2009): Nystrom discretization of parabolic boundary integral equations, *Appl. Numer. Math.* 59 (11), 2843–2856.

von Estorff, O.; Rjasanow, S.; Stolper, M.; Zaleski, O. (2005): Two efficient methods for a multifrequency solution of the helmholtz equation, *Comput. Vis. Sci* 8 (3-4), 159–167.